Structural Insights into the β-Mannosidase from *T. reesei* Obtained by Synchrotron Small-Angle X-ray Solution Scattering Enhanced by X-ray Crystallography†

Ricardo Aparicio,‡ Hannes Fischer,§ David J. Scott,# Koen H. G. Verschueren,⊥,$ Anna A. Kulminskaya,|| Elena V. Eneiskaya,|| Kirill N. Neustroev,|| Aldo Felix Craievich,§ Alexander M. Golubev,|| and Igor Polikarpov*,&

Instituto de Física Gleb Wataghin, Universidade Estadual de Campinas, Campinas, SP, Brazil, Instituto de Física, Universidade de São Paulo, São Paulo, SP, Brazil, Department of Biochemistry, School of Medical Sciences, University of Bristol, Bristol, United Kingdom, Structural Biology Laboratory, Department of Chemistry, University of York, York, United Kingdom, Petersburg Nuclear Physics Institute, Gatchina, St. Petersburg, Russia, and Instituto de Física de São Carlos, Universidade de São Paulo, São Carlos, SP, Brazil

Received March 14, 2002; Revised Manuscript Received May 16, 2002

ABSTRACT: A molecular envelope of the β-mannosidase from *Trichoderma reesei* has been obtained by combined use of solution small-angle X-ray scattering (SAXS) and protein crystallography. Crystallographic data at 4 Å resolution have been used to enhance informational content of the SAXS data and to obtain an independent, more detailed protein shape. The phased molecular replacement technique using a low resolution SAXS model, building, and refinement of a free atom model has been employed successfully. The SAXS and crystallographic free atom models exhibit a similar globular form and were used to assess available crystallographic models of glycosyl hydrolases. The structure of the β-galactosidase, a member of a family 2, clan GHA glycosyl hydrolases, shows an excellent fit to the experimental molecular envelope and distance distribution function of the β-mannosidase, indicating gross similarities in their three-dimensional structures. The secondary structure of β-mannosidase quantified by circular dichroism measurements is in a good agreement with that of β-galactosidase. We show that a comparison of distance distribution functions in combination with 1D and 2D sequence alignment techniques was able to restrict the number of possible structurally homologous proteins. The method could be applied as a general method in structural genomics and related fields once protein solution scattering data are available.

β-mannosidase (β-D-mannoside mannohydrolase, EC 3.2.1.25) is an exoglycosidase that catalyzes hydrolysis of nonreducing residues of β-D-mannose in β-D-mannosides. The enzyme participates in several biological processes, of which lysosomal degradation of N-glycoproteins is probably the most important one. Glycoprotein degradation occurs predominantly within cell lysosomes by the sequential action of endo- and exoglycosidases. β-Mannosidase cleaves mannosidic bonds in the core part of N-linked glycans attached to glycoproteins (*1*). In humans and ruminants, a deficiency of β-mannosidase leads to an autosomal recessive inherited lysosomal storage disease (*2*) called β-mannosidosis. In the case of man, clinical manifestations are heterogeneous and include mental retardation, peripheral neuropathy, and skeletal abnormalities (*3*). Fungi and bacteria that are able to degrade hemi cellulose also secrete β-mannosidase. Fungal and bacterial β-mannosidases hydrolyze β(1−4)-D-mannosyl groups from manno-oligosaccharides and mannose-containing glycopeptides that are produced from the hemi cellulose pulp by endoenzymes (*4*). In seeds that have galactomannans as storage carbohydrates, the enzyme converts manno-oligosaccharides to monosaccharides (*5*).

β-mannosidase from *Trichoderma reesei* is an extracellularly secreted 105 kDa glycoprotein (*6*). Kinetic studies proved the existence in *T. reesei* β-mannosidase of a noncatalytic galactomannan-binding site (*6*). Although the precise role of this site is not clear, this result might suggest that the β-mannosidase fold is comprised of more than one domain. To provide experimental structural information about *T. reesei* β-mannosidase, X-ray crystallographic (*7*), circular dichroism (CD), and small-angle X-ray scattering (SAXS) studies were initiated. In work presented here, a low-resolution envelope of the protein was retrieved by an ab initio procedure from the synchrotron SAXS[1] data. The envelope was further improved with the aid of higher

† This work was supported by Fundação de Amparo à Pesquisa do Estado de São Paulo (FAPESP), Brazil, via Grants 98/06761-1, 99/09471-7, 00/03387-4, and Grant 00-04-48878 of Russian Foundation of Basic Research.

* To whom correspondence should be addressed: Instituto de Física de São Carlos, Universidade de São Paulo, CP 369, 13560-970, São Carlos, SP, Brazil. Phone: +55 16 273 9874. Fax: +55 16 273 9881. E-mail: ipolikarpov@if.sc.usp.br.

‡ Universidade Estadual de Campinas.

§ Instituto de Física, Universidade de São Paulo.

University of Bristol.

⊥ University of York.

& Instituto de Física de São Carlos, Universidade de São Paulo.

$ Current address: Division of Molecular Carcinogenesis, Netherlands Cancer Institute, Plesmanlaan 121, 1066 CX Amsterdam, The Netherlands.

|| Petersburg Nuclear Physics Institute, Gatchina, St. Petersburg, 188300, Russia.

[1] Abbreviations: SAXS, small-angle X-ray scattering; CD, circular dichroism; 1D, one-dimensional; 2D, two-dimensional; SAD, single wavelength anomalous dispersion; ASU, asymmetric unit; NCS, noncrystallographic symmetry.

10.1021/bi025811p CCC: $22.00
Published on Web 07/04/2002

resolution data derived from the crystallographic experiments. Information obtained from solution X-ray scattering experiments is limited by the inherent low resolution of this technique as compared to X-ray crystallographic data. The number of Shannon channels (*8*, *9*) $N_s = D_{max}S_{max}/\pi$ in the available SAXS experimental data is equal to 13. To enhance the informational content and thus improve the accuracy of the molecular envelope, we employed X-ray crystallographic data up to 4.0 Å resolution for which the equivalent number of Shannon channels would be equal to 60. Theoretical distance distribution functions were computed from the available crystallographic models of glycosyl hydrolases and compared with the experimentally derived data. Independently, the glycosyl hydrolase crystallographic models were fitted into the experimental molecular envelope. On the basis of these results and the evidence from 2D sequence alignment (*10*) and CD spectra, we propose that β-mannosidase has a molecular fold similar to the one of β-galactosidase, a member of family 2, clan GHA.

MATERIAL AND METHODS

Materials and Protein Purification. β-Mannosidase was purified to homogeneity from culture filtrate of *T. reesei* as described in ref *6*. Crystallization solutions and buffers were prepared using chemicals of an analytical grade purchased from Sigma Chemicals.

Circular Dichroism Spectroscopy. Circular dichroism spectra were acquired in-house on a J715 spectropolarimeter (Jasco Corp., Japan). The protein at a concentration of 0.3 mg/mL was placed in a 10-mm path-length cuvette. The sample chamber was purged with dry nitrogen to remove oxygen from the optical path. Spectra were obtained in sodium acetate 50 mM buffered at pH 4.7, and spectra for the buffer were subtracted from those for the β-mannosidase samples.

Secondary structure content was analyzed using the neural net program K2D (*11*). Data were submitted online to the DichroWeb website (http://www.cryst.bbk.ac.uk/cdweb/html/home.html) via the online submission procedure (*12*). Data over the range 200−241 nm was used. The determined NRMSD goodness of Fit parameter (*13*) was found to be 0.143.

Small-Angle X-ray Scattering Experiments and Data Analysis. β-Mannosidase samples with the concentration 4 mg/mL were prepared in 50 mM sodium acetate buffer (pH 4.7). X-ray solution scattering data were collected at 4 °C with the low-angle scattering camera at the station 2.1 (*14*) at the Daresbury Synchrotron Radiation Source using a 200 × 200 mm position-sensitive multiwire proportional counter operated at 512 × 512 pixel mode (*15*). At a sample-to-detector distance of 2 m and an X-ray wavelength λ of 1.54 Å, a momentum transfer q interval of 0.03−0.35 Å^{-1} was covered ($q = 4\pi \sin\theta/\lambda$, θ being half of the scattering angle). The q range was calibrated using an oriented specimen of wet rat tail collagen (based on a diffraction spacing of 670 Å). The sample was held in a temperature-controlled brass cell containing a Teflon ring sandwiched by two mica windows. The cell has a sample volume of 120 μL and a thickness of 1.5 mm. Buffer and sample SAXS data were collected alternatively, each in frames of 60 s. The systematic data reduction included radial integration of the two-dimensional images, normalization of the subsequent one-dimensional data to the intensity of the transmitted beam, correction for detector artifacts, and subtraction of background scattering from the buffer (subtraction of the scattering from the camera and a cell filled with buffer). Data reduction was performed with the OTOKO software package (*16*), modified, and adapted for the Daresbury NCD software suite. Scattering data analysis was followed by standard procedures (*17*). Using the indirect Fourier transform method as implemented in the program GNOM (*18*, *19*), the intraparticle distance distribution function p(r), the radius of gyration of the protein, Rg, using Guinier law (*20*), and integral properties of p(r) and the extrapolated forward scattering intensity, $I(q = 0)$ (in a relative scale), were determined from the experimental scattering data.

Ab Initio Molecular Shape Determination from SAXS Experiments. The scattering intensity function was determined in 90 frames, 60 s each. Since the scattering intensity from 0.10 up to 0.35 Å^{-1} did not vary with time, all frames were used to construct it in this q range. Because of radiation-induced aggregation effects on the scattering intensity, only the first frame was used to compose the scattering curve in the low-q range.

The resolution of the resulting solution X-ray scattering curve extended to 18 Å. The low resolution particle shape was restored using the ab initio procedure described by Svergun (*21*) as implemented in the program GASBOR. In this method, a dummy residue (DR) model is generated by a random-walk C_α chain and is folded in such a way to minimize a discrepancy between the calculated scattering curve from the model and the experimental data. The program simulates the protein internal structure, which makes it unnecessary to subtract a constant background from the experimental data to ensure the asymptotic Porod's behavior (*22*). Several runs of ab initio shape determination with different starting conditions lead to consistent results as judged by the structural similarity of the output models, yielding nearly identical scattering patterns and fitting statistics in a stable and self-consistent process. The final shape restoration was performed using 950 dummy residues and 611 waters assuming no molecular symmetry. The resulting 18 Å resolution structure was used to calculate a low resolution envelope of the protein.

Enhancement of SAXS Envelope by using Crystallographic Data. T. reesei β-mannosidase was crystallized in the presence of $CdCl_2$ as described (*7*). Crystals diffracting to medium resolution (∼2.5 Å) grow in space groups $P4_12_12$ and $P2_12_12_1$ under very similar crystallization conditions. Both crystal forms have nearly identical cell dimensions ($a = b \cong 165$ Å and $c \cong 121$ Å) and a similar solvent content (∼70%). The asymmetric unit (ASU) of $P4_12_12$ crystal form contains 1 molecule and crystals belonging to the $P2_12_12_1$ contain 2 molecules/ASU. Due to very low homology with proteins whose structures are known, ab initio crystallographic methods have been considered for structure solution. A severe nonisomorphism problem prevented the use of the multiple isomorphous replacement (MIR) method. Anomalous signals from cadmium ions that were present in the crystallization solution allowed the use of the single-wavelength anomalous dispersion (SAD) approach. Initial SAD electron density maps were obtained in the space group $P4_12_12$ and were improved by density modification tech-

niques. Diffraction patterns of β-mannosidase are highly anisotropic in both crystal forms. Although the quality of final electron density maps was not good enough to build a crystallographic model, it was sufficient to determine the overall protein shape by the procedure described bellow.

The calculated electron density maps exhibit a clear protein/solvent boundary, but to distinguish the limits between two protein molecules by visual inspection proved to be difficult. Nevertheless, we were able to determine the correct position of a single molecule in the unit cell of a native crystal belonging to space group $P4_12_12$ using the GASBOR model obtained from SAXS experiments and initial SAD phases. The phased molecular replacement technique (*23*), as implemented in program AmoRe (*24*), was used for this purpose. The use of FSEARCH (*25*) was computationally prohibitively expensive due to the absence of molecular and noncrystallographic symmetry in space group $P4_12_12$. The molecular replacement solution was modified by a cyclic use of Arp warp (*26*, *27*) and Refmac (*28*), in a procedure similar to that described in Sabini (*29*). Data extending up to 2.5 Å were included. The process was interrupted when the Free R-factor stopped decreasing; the initial and final values were about 56 and 45%, respectively. The final model contains 4800 free atoms and, because of the poor quality of the available phase information, reflects only the overall shape of the protein as observed in the electron density map.

Further evidence of the accuracy of the final model obtained using electron density maps in space group $P4_12_12$ was found. First, this model was used successfully for molecular replacement in crystals from space group $P2_12_12_1$, for which no previous phase information was available. Despite the fact that β-mannosidase is a monomer in solution, this space group contains two molecules in the asymmetric unit related by a rotation of 90° (as obtained by calculating the self-rotation function map). Molecular replacement solution was unequivocal, with a correlation coefficient of 65.5% after rigid body refinement. Second, a later comparison of crystal packing in both space groups showed that almost exactly the same dimer is generated by applying crystallographic symmetry operations to the free atom model obtained in space group $P4_12_12$. Moreover, the symmetry relating the two molecules in ASU of space group $P2_12_12_1$ is pseudo-crystallographic and is equivalent to the 4-fold screw axis from space group $P4_12_12$.

Third, phases calculated from the resulting dimer in the space group $P2_12_12_1$ were used to compute anomalous difference maps (as mentioned above, crystals grow in the presence of cadmium ions in both space groups), leading to reliable identification of the heavy atom sites. Nevertheless, this crystal form presents the same problems observed for $P4_12_12$ crystals, and the resulting electron density maps were not interpretable even with a help of putative homologous structures (see Discussion) and were not used for further model building.

Fourth, a number of sites found in space group $P2_12_12_1$ by using the anomalous maps were recognized to be previously found by Patterson methods in early attempts to solve the phase problem. Moreover, a number of heavy atoms were found to bind to the same sites of the protein in both space groups, while some other sites are present exclusively in only one space group, which is probably related to packing changes from one space group to the other. And last but not least, electron density maps obtained in space group $P2_12_12_1$ from refinement of heavy atom parameters are in complete agreement with the cell volume occupied by the protein model resulting from molecular replacement procedure.

In short, the procedure for enhancement of the protein envelope included the use of the SAXS envelope and additional crystallographic information. SAXS results combined with available crystallographic data allowed for the location of the molecule inside the unit cell and for the determination of another envelope with a better resolution than that exclusively inferred from SAXS results.

Alignment Procedures and Envelopes Composition. The superposition of crystallographic structures and free atom models was done using the program SUPCOMB (*30*). To keep the original low-resolution limit of the SAXS data, envelopes (masks) were computed from coordinate files output by GASBOR using NCSMASK (*26*, *27*). For SAXS models, the NCSMASK parameter "radius", which sets the sphere radius for building the mask out of the model atoms, was adjusted to 5.7 Å to remove all internal characteristics and the parameter "smooth" was set to 18.0 Å to eliminate features smaller than 18.0 Å from the surface of the mask. To obtain masks for the crystallographic model, NSCMASK was used with both parameters set to 4.0 Å to take into account only the shape of the protein. As this model contains about 4800 atoms and was obtained using X-ray data to 4.0 Å resolution, the use of a smaller sphere radius was sufficient to eliminate internal characteristics. Atomic models derived p(r) functions were calculated using CRYSOL (*31*). Following a standard procedure, all waters from crystallographic models were removed, and a 3 Å hydration layer was added prior to p(r) function computation.

RESULTS

Overall Dimensions and Shape of β-Mannosidase. The scattering curve obtained as described in Materials and Methods and the Guinier plot are presented in Figure 1. The Guinier plot exhibits a linear behavior within the interval of $0.03\ \text{Å}^{-1} < q < 0.08\ \text{Å}^{-1}$, from which a radius of gyration of 35.6 ± 0.2 Å was calculated (*20*). The pair distribution functions p(r) computed for the SAXS and crystallographic molecular models are shown in Figure 2. The function obtained from SAXS low-resolution model indicates a maximum dimension of the molecule $d_{max} = 120 \pm 10$ Å. The peak is centered at 42 Å indicating that the particle has a prolate shape. As can be seen in Figure 2, the same maximum molecular dimension is inferred from the p(r) function corresponding to the model derived using crystallographic data. This function fits well with the p(r) function obtained from SAXS results up to about 40 Å and is lower between 40 and 120 Å. This last result indicates that the crystallographic model leads to an envelope in which large dimensions in some regions are smaller than those of the SAXS model. This is confirmed by the pictures shown in Figure 3. The overall shapes of the models are in good agreement. They are composed of a globular structural core extending continuously toward a smaller and narrower portion, probably as an indication of a multidomain structure. The main differences occur in particular surface areas where the SAXS model extends into the solvent more than the

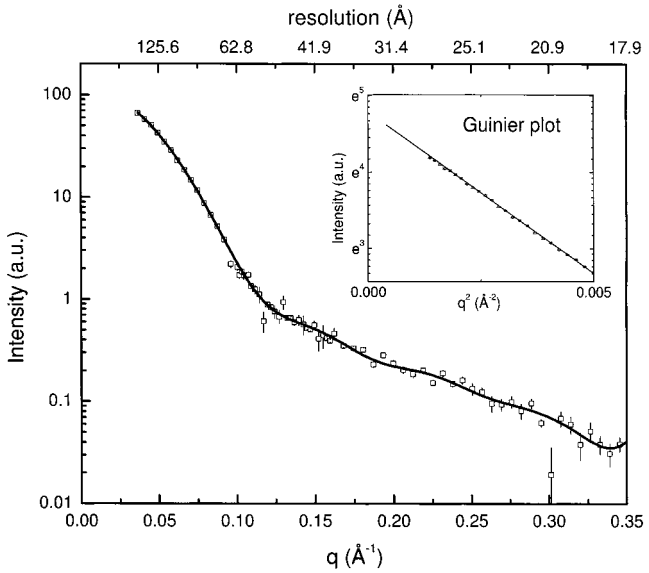

FIGURE 1: Experimental and calculated small-angle X-ray solution scattering of β-mannosidase. Experimental solution scattering curve (squares with error bars) was obtained as described in the text. The Guinier plot with linear fit is shown in the inset yielding to a radius of gyration of 35.6 ± 0.2 Å. The smooth curve is the corresponding scattering curve obtained from the dummy residue model derived by GASBOR, χ of fitting is 1.55.

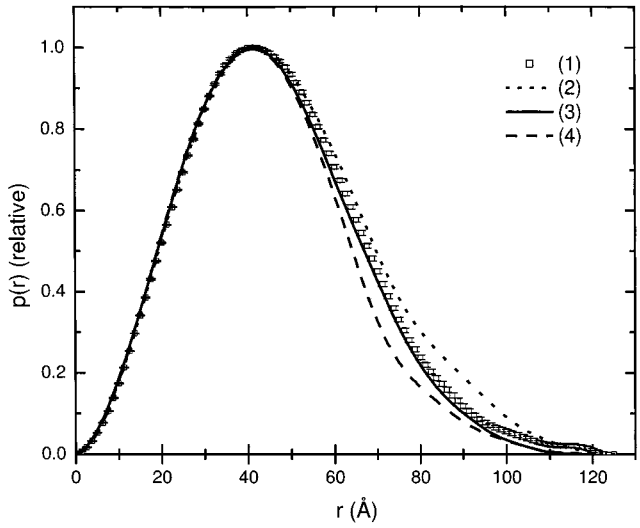

FIGURE 2: Distance distribution functions *p*(r). The curve obtained from experimental scattering curve (1; open squares) was calculated using program GNOM. Corresponding curves evaluated for β-galactosidases from *E. coli* (2; dotted line) and *Penicillium* sp. (3; solid line) and for the envelope enhanced by using X-ray crystallographic data (4; dashed line) are shown. *p*(r) functions are normalized to the maximum of each curve individually. For further details, see the text.

crystallographic model, probably as an effect of the intrinsic low resolution of SAXS data or as a consequence of the protein glycosilation. As expected, more structural details can be seen in the envelope enhanced by crystallographic data.

DISCUSSION

The Putative β-Mannosidase Fold. A number of glycosyl hydrolases with molecular masses around 100 kDa were considered as possible templates for β-mannosidase from *T. reesei*. A good fit to the *p*(r) function calculated from the

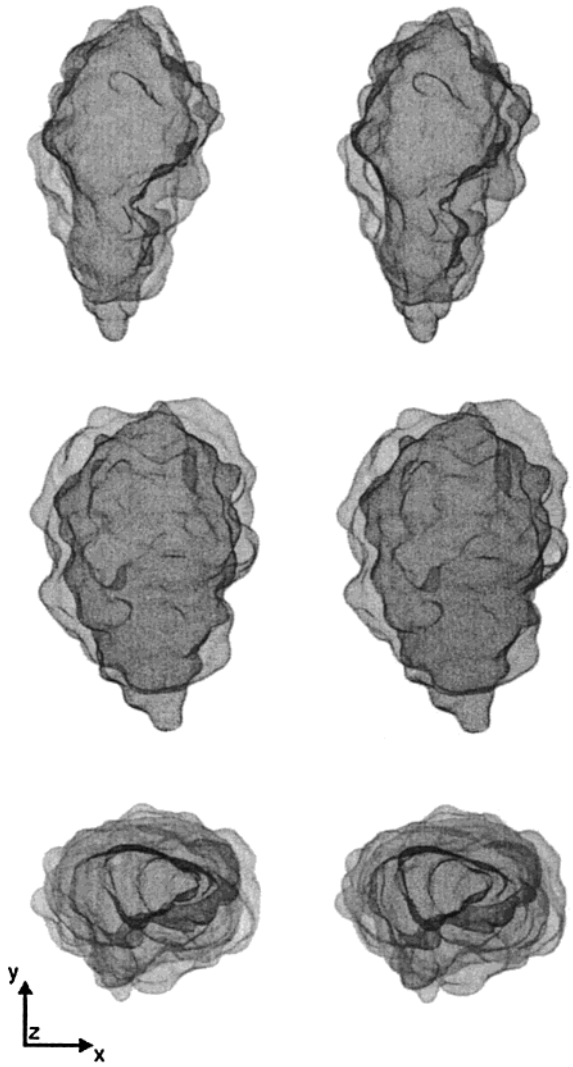

FIGURE 3: Stereoviews of β-mannosidase envelopes. The semi-transparent envelope in gray represents the dummy residue model derived by GASBOR using only SAXS data. The envelope in black represents the more detailed model, enhanced by using X-ray crystallographic data. The middle and bottom rows are rotated clockwise by 90° around the y-axes and counterclockwise by 90° around x-axes, respectively. See text for further details. Drawings were made using PyMOL (DeLano Scientific, San Carlos, CA, http://www.pymol.org) under Linux.

free atom model was obtained with the family 2 glycosyl hydrolase β-galactosidase from *Escherichia coli* (*32*), which will be referred to as 1BGLa (PDB entry 1BGL, chain A). The *p*(r) function calculated for 1BGLa, shown in Figure 2, coincides with *p*(r) functions calculated for the SAXS and crystallographic free atom models up to 60 and 40 Å, respectively, and has the same maximum dimension of 120 Å. This is a surprisingly good fit in view of expected structural divergence between β-galactosidase and β-mannosidase, differences in the glycosylation state, and the higher molecular weight of the former.

β-Galactosidase from *E. coli* has a TIM-barrel-like core surrounded by four other largely β domains. A ribbon representation of 1BGLa superposed onto the surface representation of the crystallographically enhanced molecular shape derived for β-mannosidase is shown in the Figure 4. This superposition suggests that the globular core of the protein possibly contains an $(\alpha/\beta)_8$ barrel and two other

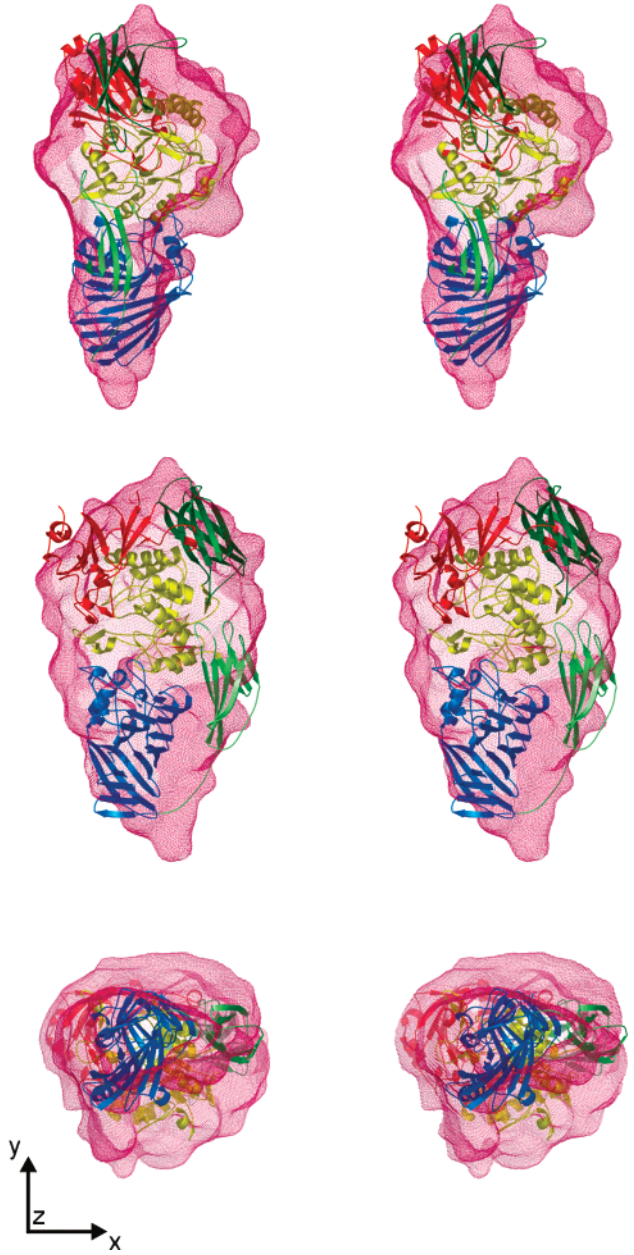

FIGURE 4: Stereoviews showing the superposition of a cartoon representation of β-galactosidase from *E. coli* (PDB entry 1BGL, chain A) on the crystallographically enhanced β-mannosidase envelope. The same perspectives of Figure 3 are shown, with middle and bottom rows rotated clockwise by 90° around the y-axes and counterclockwise by 90° around x-axes, respectively. The clipping plane allows for an inside view of envelope contents. Domains 1, 2, 3, 4, and 5 of the β-galactosidase monomer are colored in red, green, yellow, lime, and blue, respectively. The domain 3 (TIM barrel) forms the core of the monomer. The other domains surrounding the core are composed mainly of β-structures. This figure was prepared using PyMOL (DeLano Scientific, San Carlos, CA, http://www.pymol.org) under Linux.

possible domains, while the narrower portion extending from the core can accommodate two more substructures. The structural similarity provides support to the hypothesis that the additional domains are composed mainly by β strands. Some of the β strands, mainly located in the 1BGLa domains 4 and 5, protrude out of the β-mannosidase envelope. They could be simply inexistent or this might be an effect of a different orientation of the domains 4 and 5, what is indicated by the empty portions seen close to those domains. This view

Table 1: Comparison of Secondary Structure Composition of β-Galactosidases from *E. coli* (PDB entry 1BGL, chain A) and *Penicillium* sp. and β-Mannosidase from *T. reesei*[a]

secondary structure composition	*E. coli* β-galactosidase	*Penicillium* sp. β-galactosidase	*T. reesei* β-mannosidase
α (%)	14	16	28
β (%)	41	39	30
others (random, turns) (%)	45	45	42

[a]As obtained by circular dichroism spectroscopy.

is supported by a comparison between 1BGLa and the structure of β-galactosidase from *Penicillium* sp., recently solved by our group (unpublished results), which has a very similar structure, where the $(\alpha/\beta)_8$ and the other four largely β domains have slightly different sizes and orientations in comparison with those corresponding in 1BGLa. The $p(r)$ function calculated from *Penicillium* sp. β-galactosidase, shown in Figure 2, is closer to the crystallographic $p(r)$ than 1BGLa. The superposition of this model to the β-mannosidase envelopes is remarkable and a striking indication that the latter has a great structural similarity with β-galactosidase from *Penicillium* sp.

Further support to our hypothesis comes from the theoretical prediction of the catalytic domain structure of bovine β-mannosidase done by Durand and collaborators (*10*). In that work, based on known three-dimensional structures from some families of clan GH-A, a group comprising more than 200 proteins sharing low sequence identity, structural and functional features shared by those proteins were deduced. Using the 2D hydrophobic cluster analysis (HCA) method (*33*), which can be applied to analyze proteins sharing very low identity (typically 15−25%, ref *34*), the authors found the probable fold as well as likely functional amino acids of the catalytic domains of five lysosomal glycosyl hydrolases from families 1, 2, 5, 10, and 17 and, in particular, bovine β-mannosidase. It was suggested that bovine β-mannosidase, which has about 65% amino acid sequence identity with β-mannosidase from *T. reesei*, could have a $(\alpha/\beta)_8$ barrel catalytic domain. Our results are in excellent agreement with this theoretical prediction. Moreover, the β-mannosidase secondary structure assessed by CD technique is in a close agreement with the secondary structure composition of β-galactosidases from both *E. coli* and *Penicillium* sp. (Table 1). This further supports our hypothesis of the close structural similarity of these proteins.

We have shown that the distance distribution functions obtained from SAXS results and crystallographic data provided insights into the arrangements of β-mannosidase domains by comparison with other known structures. We believe that this approach combined with molecular modeling and bioinformatics techniques may be applied as a general tool in protein shape recognition. Although it cannot provide a unique solution in search for protein fold, this method is able to restrict the possible folding space of an unknown protein once solution scattering data and its secondary structure composition obtained for example by CD or infrared spectroscopy are available. This method provides an information independent of the protein amino acid sequence based on the 1D and 2D alignment algorithms. The proposed procedure seems particularly useful within a scope of

structural genomics programs, particularly for application to poorly crystallizable proteins. Use of SAXS models for molecular replacement when initial phase information is available could also be extended to difficult cases in protein crystallography, when model building proves to be a problem. In addition, we have shown that low-resolution models derived from X-ray solution scattering experiments can actually be improved by addition of low-resolution crystallographic data.

REFERENCES

1. Scriver, C. R., Beaudet, A. L., Sly, W. S., and Valle, D. (1989) *The Metabolic Basis of Inherited Disease*, Vol. II, 6th ed., McGraw-Hill, Inc., USA.
2. Watts, R. W. E., and Gibbs, D. A. (1986) *Lysosomal Storage Diseases − Biochemical and Clinical Aspects*, Taylor & Francis, Inc., Philadelphia, USA.
3. Rodriguez-Serna, M., Botella-Estrada, R. M. D., Chabas, A., Coll, M., Oliver, V., Febrer, M., and Aliaga, A. (1996) Angiokeratoma corporis diffusum associated with beta-mannosidase deficiency. *Arch. Dermatol. 132* (*10*), 1219−1222.
4. Kuhad, R. C., Singh, A., and Eriksson, K. L. (1997) Microorganisms and enzymes involved in the degradation of plant fiber cell walls. *Biochem. Eng. Biotechnol. 57*, 45−125.
5. Dey, P. M., and del Campillo, E. (1984) Biochemistry of the multiple forms of glycosidases in plants. *Adv. Enzymol. Relat. Areas Mol. Biol. 56*, 141−249.
6. Kulminskaya, A. A., Eneiskaya, E. V., Isaeva-Ivanova, L. S., Savel'ev, A. N., Sidorenko, I. A., Shabalin, K. A., Golubev, A. M., and Neustroev, K. N. (1999) Enzymatic activity and beta-galactomannan binding property of beta-mannosidase from *Trichoderma reesei*. *Enzyme Microb. Technol. 25* (*3*−*5*), 372−377.
7. Aparicio, R., Eneiskaya, E. V., Kulminskaya, A. A., Savel'ev, A. N., Golubev, A. M., Neustroev, K. N., Kobarg, J., and Polikarpov, I. (2000) Crystallization and preliminary X-ray study of beta-mannosidase from *Trichoderma reesei*. *Acta Crystallogr. D 56*, 342−343.
8. Shannon, C. E., and Weaver, W. (1949) *The Mathematical Theory of Communication*, University of Illinois Press, Urbana.
9. Moore, P. B. (1980) Small-angle scattering. Information content and error analysis. *J. Appl. Crystallogr. 13*, 168−175.
10. Durand, P., Lehn, P., Callebaut, I., Fabrega, S., Henrissat, B., and Mornon, J. P. (1997) Active-site motifs of lysosomal acid hydrolases: invariant features of clan GH-A glycosyl hydrolases deduced from hydrophobic cluster analysis. *Glycobiology 7* (*2*), 277−284.
11. Andrade, M. A., Chacon P., Merelo, J. J., and Moran, F. (1993) Evaluation of secondary structure of proteins from UV circular dichroism using an unsupervised learning neural network. *Protein Eng. 6*, 383−390.
12. Lobley, A., Whitmore, L., and Wallace, B. A. (2002) DICHROWEB: an interactive website for the analysis of protein secondary structure from circular dichroism spectra. *Bioinformatics 18*, 211−212.
13. Mao, D., Wachter, E., and Wallace B. A. (1982) Folding of the mitochondrial proton adenosinetriphosphatase proteolipid channel in phospholipid vesicles. *Biochemistry 21* (*20*), 4960−4968.
14. Towns-Andrews, E., Berry, A., Bordas, J., Mant, G. R., Murray, P. K., Roberts, K., Sumner, I., Worgan, J. S., Lewis, R., and Gabriel, A. (1989) Time-resolved X-ray diffraction station: X-ray optics, detectors, and data acquisition. *Rev. Sci. Instrum. 60*, 2346−2349.
15. Lewis, R. (1994) Multiwire gas proportional counters: decrepit antiques or classic performers? *J. Synchrotron Rad. 1*, 43−53.
16. Boulin, C., Kempf, R., Koch, M. H. J., and McLaughlin, S. M. (1986) Data appraisal, evaluation and display for synchrotron radiation experiments − hardware and software. *Nucl. Instrum. Methods Phys. Res. A249*, 399−407.
17. Grossmann, J. G., Crawley, J. B., Strange, R., Patel, K. J., Murphy, L. M., Neu, M., Evans, R. W., and Hasnain, S. S. (1998) The nature of ligand-induced conformational change in transferrin in solution. An investigation using X-ray scattering, XAFS and site-directed mutants. *J. Mol. Biol. 279*, 461−472.
18. Svergun, D. I., Semenyuk, A. V., and Feigin, L. A. (1988) Small-angle-scattering-data treatment by the regularization method. *Acta Crystallogr. A 44*, 244−251.
19. Svergun, D. I. (1992) Determination of the regularization parameter in indirect-transform methods using perceptual criteria. *J. Appl. Crystallogr. 25*, 495−503.
20. Guinier, A., and Fournet, G. (1955) *Small-Angle Scattering of X-rays*, John Wiley & Sons, New York.
21. Svergun, D. I., Petoukhov, M. V., and Koch, M. H. J. (2001) Determination of Domain Structure of Proteins from X-ray Solution Scattering. *Biophys. J. 80*, 2946−2953.
22. Porod, G. (1982) *General Theory in Small-Angle X-ray Scattering*, (Glatter, O., and Kratky, O., Eds.) pp 17−51, Academic Press, London.
23. Bentley, G. A. (1992) Some applications of the phased translation function using calculated phases in Molecular Replacement, *Proceedings of the Daresbury Study Weekend*, DL/SCI/R33.
24. Navaza, J. (1994) AMoRe: an automated package for molecular replacement. *Acta Crystallogr. A50*, 157−163.
25. Hao, Q. (2001) Phasing from an envelope. *Acta Crystallogr. D 57*, 1410−1414.
26. Collaborative Computational Project (1994) No. 4, *Acta Crystallogr. D 50*, 760−763.
27. Winn, M., Dodson, E. J., and Ralph, A. (1997) Collaborative Computational Project, Number 4: Providing Programs for Protein Crystallography. *Methods Enzymol. 277*, 620−633.
28. Murshudov, G. N., Vagin, A. A., and Dodson, E. J. (1997) Refinement of Macromolecular Structures by the Maximum-Likelihood Method. *Acta Crystallogr. D 53*, 240−255.
29. Sabini, E., Schubert, H., Murshudov, G., Wilson, K. S., Siika-Aho, M., and Penttilä, M. (2000) The three-dimensional structure of a *Trichoderma reesei* beta-mannanase from glycoside hydrolase family 5. *Acta Crystallogr. D 56*, 3−13.
30. Kozin, M. B., and Svergun, D. I. (2001) Automated matching of high- and low-resolution structural models, *J. Appl. Crystallogr. 34*, 33−41.
31. Svergun, D., Barberato, C., and Koch, M. H. J. (1995) CRYSOL − a Program to Evaluate X-ray Solution Scattering of Biological Macromolecules from Atomic Coordinates, *J. Appl. Crystallogr. 28*, 768−773.
32. Jacobson, R. H., Zhang, X. J., DuBose, R. F., and Matthews, B. W. (1994) Three-dimensional structure of beta-galactosidase from *E. coli*. *Nature*, *369* (*6483*), 761−766.
33. Gaboriaud, C., Bissery, V., Benchetrit, T., and Mornon, J. P. (1987) Hydrophobic cluster analysis: an efficient new way to compare and analyse amino acid sequences. *FEBS Lett. 224*(*1*), 149−55.
34. Lemesle-Varloot, L., Henrissat, B., Gaboriaud, C., Bissery, V., Morgat, A., and Mornon, J. P. (1990) Hydrophobic cluster analysis: procedures to derive structural and functional information from 2-D-representation of protein sequences. *Biochimie 72*(*8*), 555−74.

BI025811P